AD-A078 796 MASSACHUSETTS UNIV AMHERST ASTRONOMY RESEARCH FACILITY F/G 7/4
INFRARED EMISSION SPECTROSCOPY OF LOW PRESSURE GASEOUS DISCHARG--ETC(U)
JUL 79 P HANSEN , H SAKAI F19628-76-C-0087
UNCLASSIFIED UMASS-ARF-79-305 AFGL-TR-79-0150 NL

| OF |
AD-
A078796

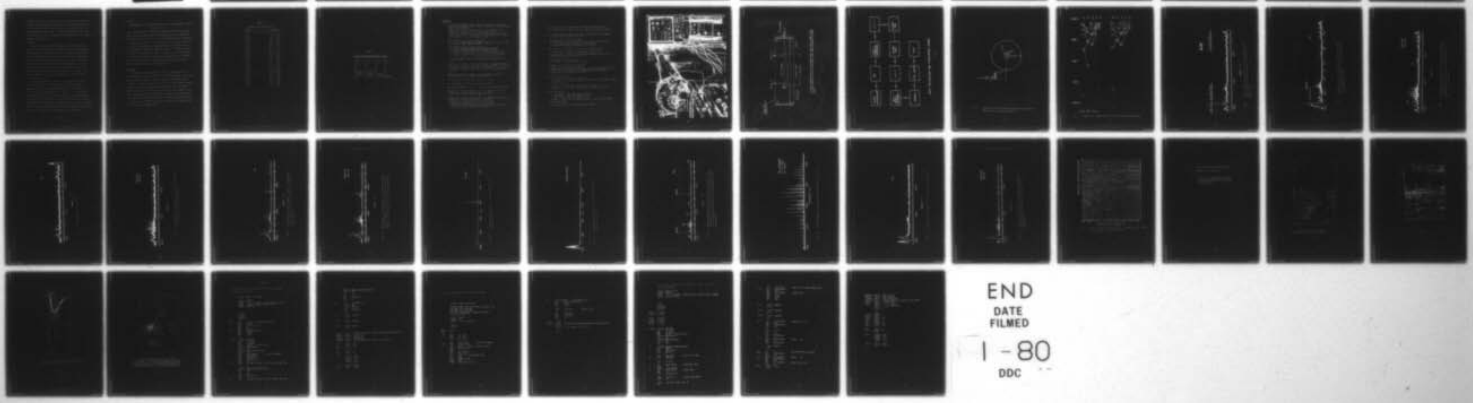

END
DATE
FILMED
1-80
DDC

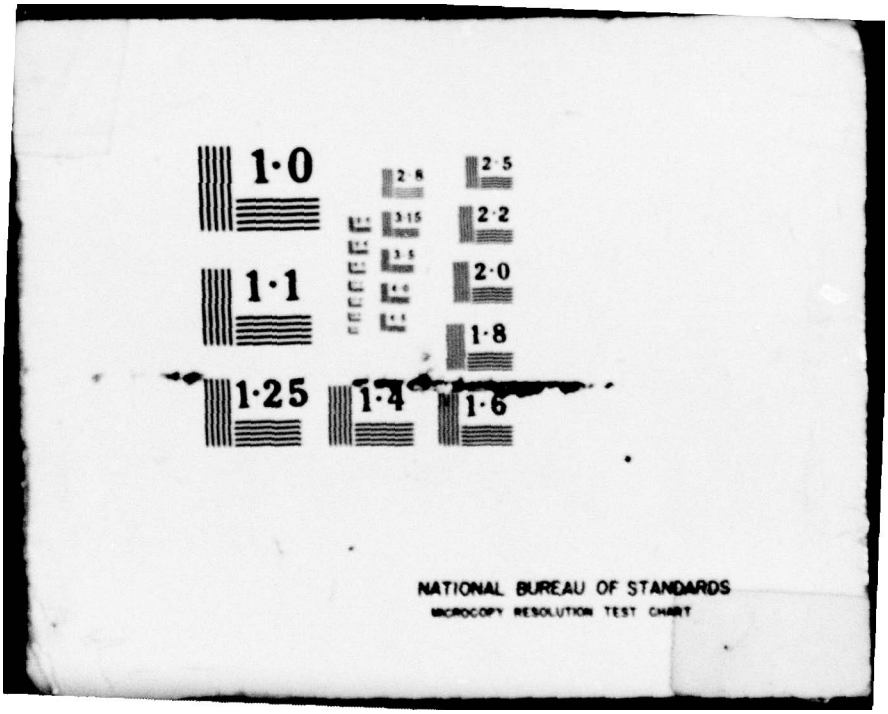
1·0
1·1
1·25
1·4
1·6
2·2
2·0
1·8
NATIONAL BUREAU OF STANDARDS
MICROCOPY RESOLUTION TEST CHART

AFGL-TR-79-0150

LEVEL II

12 SC

AD A051135

AD A078796

INFRARED EMISSION SPECTROSCOPY OF LOW PRESSURE GASEOUS DISCHARGES, II

Peter Hansen
Hajime Sakai

Astronomy Research Facility
University of Massachusetts
Amherst, MA 01003

10 July 1979

Scientific Report No. 2

Approved for public release; distribution unlimited.

AIR FORCE GEOPHYSICS LABORATORY
AIR FORCE SYSTEMS COMMAND
UNITED STATES AIR FORCE
HANSCOM AFB, MASSACHUSETTS 01731

UNCLASSIFIED

SECURITY CLASSIFICATION OF THIS PAGE (When Data Entered)

REPORT DOCUMENTATION PAGE

READ INSTRUCTIONS BEFORE COMPLETING FORM

1. REPORT NUMBER: AFGL-TR-79-0150	2. GOVT ACCESSION NO.
3. RECIPIENT'S CATALOG NUMBER	
4. TITLE (and Subtitle): INFRARED EMISSION SPECTROSCOPY OF LOW PRESSURE GASEOUS DISCHARGES, II.	5. TYPE OF REPORT & PERIOD COVERED: Interim Scientific Report No. 2
	6. PERFORMING ORG. REPORT NUMBER: UMASS-ARF-79-305
7. AUTHOR(s): Peter Hansen, Hajime Sakai	8. CONTRACT OR GRANT NUMBER(s): F19628-76-C-0087
9. PERFORMING ORGANIZATION NAME AND ADDRESS: Astronomy Research Facility, University of Massachusetts, Amherst, MA 01003	10. PROGRAM ELEMENT, PROJECT, TASK AREA & WORK UNIT NUMBERS: 61102F; 2310G405; G4
11. CONTROLLING OFFICE NAME AND ADDRESS: Air Force Geophysics Laboratory, Hanscom AFB, Massachusetts 01731, Monitor/Alastair Fairbairn/OPR	12. REPORT DATE: 10 July 1979; 50
	13. NUMBER OF PAGES: 49
14. MONITORING AGENCY NAME & ADDRESS (if different from Controlling Office): UMASS-ARF-79-305, SCIENTIFIC-2	15. SECURITY CLASS. (of this report): Unclassified
	15a. DECLASSIFICATION/DOWNGRADING SCHEDULE

16. DISTRIBUTION STATEMENT (of this Report)

Approved for public release; distribution unlimited.

17. DISTRIBUTION STATEMENT (of the abstract entered in Block 20, if different from Report)

18. SUPPLEMENTARY NOTES

19. KEY WORDS (Continue on reverse side if necessary and identify by block number)

Emission spectra
Fourier spectroscopy
Gaseous discharge
Infrared

20. ABSTRACT (Continue on reverse side if necessary and identify by block number)

This report summarizes a survey study aimed at improving our understanding of the physical processes which control the infrared radiation in the upper atmosphere. The experiment is conducted to generate various infrared bands of the atmospheric species in our large discharge chamber. Interpretations are given for the observed data by identifying the species involved and determining their parameters in terms of the atomic or molecular transitions.

DD FORM 1 JAN 73 1473

UNCLASSIFIED

406 989

INFRARED EMISSION SPECTROSCOPY OF LOW PRESSURE GASEOUS DISCHARGES

This program is a laboratory study aimed at improving our understanding of the physical processes which control the infrared radiation in the upper atmosphere.[1] Our effort is to generate various infrared bands of the atmospheric species in our large discharge chamber. We interpret the observed data by identifying the species involved and determining their parameters in terms of the atomic or molecular transitions.[2]

Our experimental approach is to use a 36-meter-long electric discharge column as an infrared emission source. Spectrometric study is performed using the technique of Fourier spectroscopy.[3] We achieve a large improvement in detection of weak infrared emission bands by combining an efficient spectrometric technique with the infrared emission source. This allows data measurement within a short time period while maintaining an adequate spectral resolution.

EXPERIMENTAL SETUP

An overall view of our large discharge source and spectrometric arrangement is shown in Fig. 1. A 30-meter-long 1-meter-diameter cylinder is used as a container of the discharge source, which is formed between a 12-meter-long central electrode and the external wall as shown in Fig. 2. An a.c. 60 Hz voltage of up to 1000 V is applied between the electrodes, activating the discharge. The interferometer accepts the infrared radiation through a KBr lens placed at the exit port of the discharge source. The interferogram signal is observed by a detector housed in a

liquid nitrogen dewar. The path difference is monitored by the interference fringe signal of the HeNe cw laser line at 6328 Å (air wavelength). The detector output is ac-amplified, synchronously demodulated, and integrated through a standard lock-in amplifier setup. The output signal of the lock-in amplifier is converted to a digital signal by an analog-to-digital converter, which is triggered by the zero-crossing position of the laser interference reference signal. The digitized interferogram signal is then recorded on a mass storage device (a floppy disk) under the control of an LSI-11 minicomputer. After completion of the interferogram measurement, the interferogram data is post-processed using our central-site large-scale computer, CDC CYBER system, for the Fourier transformation, etc. Our data acquisition scheme is shown schematically in Fig. 3. The programs for the LSI-11 data acquisition process and the data transfer to CYBER are included in this report (see Appendix). These programs are incorporated with version V02C-02 of the RT-11 operating system.[4]

1. Source

The optical cell shown in Fig. 2 is known as the "Pfund" cell.[5] The discharge column formed between the electrodes is seen thrice along the optical path, thus forming an equivalent 36-meter-long discharge column.

The excitation energy released to the atoms and molecules in the glow discharge can be estimated in the following way: The electric field in the cell is given as a function of a distance r, measured from the center by

$$E = \frac{V}{r(\ln\frac{b}{a})} \qquad (1)$$

where V is the electric potential applied between the central electrode of radius a and the wall of radius b. Fig. 4 shows a section of our cell,

which is characterized by a = 3.75 cm and b = 50 cm. In the electric field, the electrons pick up their energy between collisions. The mean free path <x> of these electrons can be given by

$$\langle x \rangle \approx \frac{1}{n\sigma} \tag{2}$$

where n is the number density of the colliding molecules and σ is the collision cross-section. If an electron moves parallel to the field direction between a collision, it increases its average kinetic energy ε by <x>eE

$$\varepsilon = e\langle x \rangle E = \frac{eV}{r(\ln\frac{b}{a})n\sigma} = \frac{eVp_o}{r(\ln\frac{b}{a})N_o p} . \tag{3}$$

It is seen that the excitation is the highest in the vicinity of the electrode and that it reduces toward the outer wall. For a typical example, we can assume $\sigma \approx 10^{-16}$ cm^2,[6] V = 700V, and $n = N_o\frac{p}{p_o} = 2.687 \times 10^{16}$ for p = 0.76 torr. The field at r = 10 cm is about 27 V/cm, while the mean free path is about 0.37 cm. The excitation at r = 10 cm would reach 10 eV = 80680 cm^{-1}. In reality, the electrons do not necessarily move parallel to the lines of Force, and the cross-section σ is dependent on the electron energy. Nonetheless, our estimate may be accepted as a rough value.

One thing noticeable is that the excitation is very sensitive to the gas pressure. Once the gas pressure is above 0.5 torr, the glow discharge which is indicative of transitions between the electronic states is confined to the vicinity of the electrodes, leaving a dark space elsewhere. For heteronuclear molecules, the infrared emission does not necessarily occur via an electronic transition. An absence of the visible glow discharge does not eliminate a possible infrared emission. However, for

homonuclear molecules, electronic transitions are necessary to produce infrared transitions.

The voltage applied to produce a glow discharge is at 60 Hz. It is obtained from the ordinary 60 Hz power, through a step-up transformer. D.C. voltages did not produce stable discharges. The central electrode is usually water-cooled.

Fig. 5 is a sketch showing the atomic oxygen (OI) energy levels[7] together with the infrared OI lines observed in our experimental setup. (The observed OI lines are listed in Table I.) The energy of these levels is referenced to the ground state of atomic oxygen $1s^2\ 2s^2\ 2p^4\ {}^3P_2$, which is located at approximately 40,000 cm^{-1} above the molecular O_2 ground state $X\ {}^3\Sigma_g^-$. With a gas pressure of 0.2 torr and 700V applied to the electrode, we can estimate the electron energy reaching a value higher than 20 eV ($\sim$160,000 cm^{-1}). This rough estimate for the electron energy in our discharge condition is well supported by the observed OI transitions.

2. Interferogram Data Acquisition Electronics

The electronics used in the interferogram acquisition scheme is a standard lock-in amplifier setup. The integration of a demodulated signal is provided by an RC filter which performs integration on the temporal axis. We have made no attempt to correct non-uniformities of the interferometer drive. As a consequence, distortion in the spectra obtained becomes pronounced whenever the interferogram data measurement extends to more than 1 cm of optical path difference.

Another problem which we did not attempt to correct is a phase mismatch between the lock-in amplifier demodulation and the excitation-relaxation sequence of various spectral components.[8] We expect that

excitations of the observable species vary in time. These species undergo their own excitation-relaxation cycle. We did not attempt to study this aspect at this moment, since a substantial modification of the electronics is needed to make a temporal separation of each evolutionary cycle. These two problems remain to be solved in the near future.

3. Interferometer

The interferometer used in this measurement is an Idealab IF-6. We used a CaF_2 beam splitter with a InSb photovoltaic detector at liquid N_2 temperature. The reference laser line was the HeNe line at 6328 Å. Some instabilities resulted in the laser's signal when the laser beam was reflected back on itself. To avoid this, the laser beam was sent slightly non-coincident with the optic axis of the interferometer. The line-position measurement consequently requires a correction of the error resulting from this tilt. The interferometer was scanned at a relatively slow speed of about 8μm/sec (13λ/sec).

SPECTRAL DATA OBTAINED AND THEIR INTERPRETATION

Our study was to inspect the infrared emission of various atmospheric species. In doing so, we formed an electric discharge column in air under an appropriate pressure and in other gas mixtures. The spectral data inspected were those of discharges formed in He, O_2, N_2, CO_2, N_2O, NH_3, and various mixtures of these gases, in addition to those produced by air. Specific mixtures were selected to produce the spectral data necessary for interpreting those features observable in the air discharge.

Fig. 6 shows the spectral feature produced in the air discharge. Because of the physical condition existing in our experimental setup as mentioned above, the data were taken at a pressure of .1 ∿ .2 torr with an

electrode voltage of 600V a.c. (rms). The current density was approximately 2×10^{-5} amp cm^{-2}, with a total power dissipation of 900 watts. In the atmosphere, pressure of 0.1 torr corresponds to an altitude near 60 km. Although temperature, excitation mechanisms and species concentration may differ somewhat, the obtained spectral features are expected to be close to those observable at that altitude. The spectra were taken with a spectral resolution of about 1 cm^{-1}. A feature observable in the lowest frequency region around 1800 cm^{-1} is the vibrational fundamental ($\Delta v = 1$) of NO ground state. The CO vibrational fundamental ($\Delta v = 1$) is the feature observable next to the NO band, followed by the CO_2 bands at 4.3μ. The feature seen between 2700 cm^{-1} and 4000 cm^{-1} consists of various electronic transitions of N_2 and the vibration fundamentals of NH and OH. The band structure above 5500 cm^{-1} belongs to the first positive system ($B^3\Pi_g$ $A^3\Sigma_u^+$) of N_2. The atomic lines of H, O and N are observable throughout the entire region covered. The atoms and molecules in the discharge chamber gain their excitation energy through the electronic collision process and emit the infrared, visible and UV radiation in the de-excitation phase. We estimated the electron energy available for the excitation to be in the order of 20 eV, as described previously. Our discussion will be on the infrared emission of these atoms and molecules in relation to excitation energy available in the electronic collision process.

For homonuclear molecules, the observable infrared transition must occur between different electronic states. The electronic transitions to the ground state involve an energy difference usually larger than 10,000 cm^{-1}, and they are observable in a region outside to the traditional infrared range. The infrared transitions are observable if the energy difference

between two respective excited states falls into a proper range. Most of these transitions involve the two highly excited states, which are very closely situated. The spectroscopic data in the visible and ultraviolet region are not helpful in furnishing a detail of those states suitable for the study of the infrared. A detail of these levels seems only possible in the infrared emission study. Unfortunately, the infrared emission study has not been intensive,[9] partially because until recently the technique was not developed to supply a good sensitivity for a meaningful measurement.

Heteronuclear molecules are infrared active in the vibrational rotational transition. Consequently, the infrared emission may be produced by the transition within the electronic ground-state without involving electronic transitions.

Fig. 7 shows the spectral feature of air discharge taken at a different time. We suspect that the air for this spectrum contains more moisture, as indicated by more distinctive NH lines. We noticed that the presence of hydrogen in the discharge column produces a significant effect on the overall excitation of various species. However, an effect of H_2O to the discharge was left unstudied at this time because we are afraid that the H_2O molecules, once they are forcefully introduced into the chamber, will irreparably contaminate the overall electrode surfaces. We introduced the H_2 into the discharge, expecting that the effect would be similar if the H_2O molecules would dissociate in the discharge excitation. With this expectation, we took data of various gases with and without H_2 mixing. The spectral data shown in Figs. 8 through 18 were collected for producing a proper identification to those spectral features observed in the air discharge data, as well as for obtaining a general insight to the

physics and chemistry of the responsible species. We were able to identify in the air discharge data those features produced by N_2, N, O_2, O, H, CO_2, CO, OH, NH, and NO. The following provides a brief description of these species.

(a) Nitrogen[10]

The spectra are shown in Fig. 9 for pure nitrogen discharge and in Fig. 10 for N_2 mixed with 30% hydrogen. It can be seen from these figures that the nitrogen molecules produce an extremely complex feature, nothing comparable to either the oxygen or the hydrogen molecules. Fig. 19 shows the molecular potential curves of various molecular nitrogen states. The lowest excited states are a group of triplet states, consisting of $A\ ^3\Sigma_u^+$, $B\ ^3\Pi_g$, $B'\ ^3\Sigma_u^-$ and $W\ ^3\Delta_u$. The ~~so-called~~ "first positive" bands of N_2 which are observable in the 7000 ~ 8000 cm^{-1} range are the transitions between $A\ ^3\Sigma_u^+$ and $B\ ^3\Pi_g$. As the molecule gets more excited, the "Benesch-Wu" bands (in the 2300 to 4000 cm^{-1} range) between $B\ ^3\Pi_g$ and $W\ ^3\Delta_u$ are formed. Other transitions which fall into the InSb region are the McFarlane infrared systems (in the 2300 cm^{-1} range) between $w\ ^1\Delta_u$ and $a\ ^1\Pi_g$, and $a\ ^1\Pi_g$ and $a'\ ^1\Sigma_u^-$.

Once the excitation reaches the next triplet group of $C\ ^3\Pi_u$, $C'\ ^3\Pi_u$ and others, its energy exceeds the dissociation limit of the ground state $X\ ^1\Sigma_g^+$. Beyond this threshold, the atomic lines would become observable. In our spectra, only few NI lines were observed. The most distinctive lines which appeared throughout the entire data are a doublet at 7444.2 cm^{-1} and 7361.0 cm^{-1} of the ($3s^2P \rightarrow 3p^2S^\circ$) transition. The dissociation energy of the ground-state N_2 is relatively high at 9 eV. Since the overall energy available for the excitation is about 20 eV, the excitation of NI

does not exceed 11 ∿ 12 eV. Consequently, we fail to observe many NI lines, in contrast to the OI case mentioned above.

(b) Oxygen[7,11]

The molecular oxygen levels sketched in Fig. 20 indicate that the molecular transitions are unlikely to be observed in the 2000 ∿ 5000 cm^{-1} region, as the O_2 molecule dissociates at a relatively low excitation energy (∿5 eV). In contrast to the N_2 case, many atomic oxygen lines are observable in the infrared as seen in the spectrum shown in Fig. 11. Table I lists major OI lines observed in the infrared region. The observable transitions indicate an overall excitation of 17 eV or higher in reference to the molecular oxygen ground state.

(c) Hydrogen

No molecular bands were observed in the data. The molecular potentials of this molecule are provided in Fig. 21 for convenience. Atomic lines are the only transitions observed in our data. Table II lists the atomic lines observed in the 2000 cm^{-1} ∿ 8000 cm^{-1} region. The overall excitation, which is a reference to the molecular hydrogen ground state, reaches 17 eV or higher. There is a notable effect of the hydrogen, either atomic or molecular, to suppression of the CO infrared fundamental transitions. We do not understand what mechanism is involved in the suppression. There are two factors to be included in considering the quenching of the CO bands. The chemical reaction rate between CO and either H_2 or H are not distinctively fast. The collision frequency is expected to increase by a factor of 10 when the hydrogen gas is introduced. The infrared CO transition is a fluorescent-type reaction which is characterized by a long radiative lifetime (longer than 1 mS). We can speculate that the

CO transition, having a long radiative lifetime, is influenced by an increased collision frequency. This is generally true for all infrared vibrational transitions occurring within the electronic ground state. An extent of this effect on the CO bands has not been fully studied for our discharge condition.

(d) $\underline{CO_2}$[12]

The excited electronic states of this molecule are vaguely known. The nearest excited state belongs to a different molecular symmetry than that of the ground state, which has a dissociation energy of 5.4 eV to a configuration of CO + O. The discharge in a pure CO_2 environment did not produce a CO_2 infrared band over the entire 1700 cm^{-1} ~ 8000 cm^{-1}. As shown in Fig. 14, the only spectral feature observed in the CO_2 discharge was the CO fundamental. There is a well known resonance between the ν_3 (0 0° 1) vibrational mode of CO_2 and the fundamental vibration of N_2. We may speculate that the CO_2 emission in the infrared is a product through a secondary process, not by a direct excitation. The spectral data taken with the CO_2/N_2 mixture, we were able to demonstrate that the ν_3 band of CO_2 increases its intensity with the N_2 concentration.

(e) $\underline{CO}$[13]

The fundamental band of this molecule is rather difficult to remove from our discharge excitation. We observed only few cases where the CO fundamental is well suppressed. The effect of hydrogen to the CO emission was described above.

(f) $\underline{OH}$[14]

The vibrational fundamental transition of this free radical was seen in most of the spectral data. The atomic lines of both O and H were

observable together with the OH band. The OH intensity was observed to increase with the hydrogen concentration. It is rather puzzling that the OH band is embarrassingly strong in the N_2/H_2 discharge data, while the NH_3 discharge data shown in Fig. 15 has no trace of the OH lines. The observed position of the OH lines shows a good agreement with the values reported by Maillard *et al.*[16]

(g) $\underline{NH}^{15}$

The NH vibrational fundamental appeared consistently in the air, N_2/H_2 and N_2O/H_2 discharge data. The NH molecules in these cases were evidently formed by recombination process. This was supported by the fact that as the hydrogen molecules were removed both the N_2 and N_2O discharges produced insignificant NH excitation. Traditionally the NH bands in the uv region were generated by decomposing NH_3. Our NH_3 discharge data were taken to identify the NH band formed both in the recombination and decomposition process, as well as to isolate it from other excitations. Fig. 16 shows the NH band taken with a spectral resolution of 0.1 cm^{-1}.

This band was somewhat unexpected, in part because there was no published infrared spectral data available and in part because the generation of the NH through recombination was not predicated at all. This free radical seems chemically more reactive to the NO than the OH, as evidenced in the result obtained in the N_2O/H_2 discharge data where the formation of the NH band is accompanied by NO emission that is much weaker than that of the pure N_2O discharge data. We conducted a thorough study on this band. The spectral analysis on this band has been completed and the results obtained will be published in the near future.

(h) NO[16]

The mechanism for forming NO molecules in the air discharge is probably:

$$N + O_2 \rightarrow NO + O,$$

as our discharge excitation creates a considerable amount of the atomic states. The NO band seen in the air discharge data must be generated by recombination, while that seen in the N_2O discharge data is by decomposition.

Comparing the spectra of Figs. 17 and 18, one for the N_2O and another for the N_2O/H_2 discharge, the NO band was seen to be suppressed in the latter spectrum as the NH band became more intense. The chemical reaction rate of NH to NO is known to be fast. At present, we do not know whether the formed NH molecules react to prevent the NO excitation or to destroy the NO molecular formation. The molecular potential curves of this molecule are provided in Fig. 23 for convenience.

CONCLUSION

A laboratory study was conducted to gain our understanding of the infrared emission spectrum observable in the upper atmosphere. In so doing, a large electric discharge column was formed in a low pressure gaseous environment. Using the technique of Fourier spectroscopy, spectral features produced by various atmospheric species were detected in the infrared emission produced in the discharge. We have gained some insight into the formation mechanism of the various emitting species, as we performed the spectrometry with a moderate resolution. Our effort was somewhat limited by two factors: an insufficient spectral resolution, and a complete lack of the time resolved spectral data.

TABLE I

Observed Atomic Oxygen Lines

(cm^{-1})	Transition
7593.7	$4s\,^3S^\circ - 3p\,^3P$
6289.5	$5d\,^5D - 4p\,^5P$
5546.9	$4f\,^5F - 3d\,^5D$
5479.4	$4f\,^3F - 3d\,^3D^\circ$
3918.9	$6f\,^5F - 4d\,^5D$
3876.2	$6f\,^3F - 4d\,^3D$
3819.9	$8s\,^5S - 5p\,^5P$
3819.9	$6g\,^3G - 4f\,^3F$
3770.7	$4d\,^5D - 4p\,^5P$
3617.2	$4p\,^5P - 4s\,^5S$
3455.4	$4p\,^3P - 4s\,^3S$
3226.9	$3d\,^3D - 4p\,^3P$
3021.9	$5s\,^5S - 4p\,^5P$
2731.0	$5s\,^3S^\circ - 4p\,^3P$
2575.7	$5f\,^5F - 4d\,^5D^\circ$
2532.7	$5f\,^3F - 4d\,^3D^\circ$
2477.3	$5g\,^5G - 4f\,^5F$
2192.1	$4p\,^3P - 3d\,^3D^\circ$
2154.6	$7g\,^5G - 5f\,^5F$
2150.5	$7f\,^5F - 5g\,^5G$

TABLE II

Observed Atomic Hydrogen Lines (cm^{-1})

n	Δn = 1	Δn = 2	Δn = 3	Δn = 4
1				
2				
3	5331.55	7799.29		
4	2467.75	3808.25	4616.53	
5		2148.79	2673.39	3033.05
6				

REFERENCES

1. A very few spectrometric studies have been conducted on the upper atmospheric infrared emission. AFGL conducted two successful measurements: SPIRE and HIRIS.
SPIRE, paper presented by Nadile *et al* at Topical Meeting on Atmospheric Spectroscopy held at Keystone,CO (1978).
HIRIS, paper presented by A.T. Stair at American Chemical Society Annual Meeting (1978), "Atmospheric Spectra Obtained by the Rocket-borne Cryogenic (10°K) Interferometer, HIRIS."

2. General reference for atomic spectroscopy:
G. Herzberg, Atomic Spectra and Atomic Structure, Second Ed., trans. by J. Spinks, Dover, New York (1944).

General reference for molecular spectroscopy:
G. Herzberg, Molecular Spectra and Molecular Structures
I. Spectra of Diatomic Molecules, Second Ed. (1950).
II. Infrared and Raman Spectra of Polyatomic Molecules (1945).
III. Electronic Spectra and Electronic Structure of Polyatomic Molecules (1966). Van Nostrand Reinhold, New York.

M. Mizushima, The Theory of Rotating Diatomic Molecules, Wiley, New York (1975).

3. G. Vanasse and H. Sakai, "Fourier Spectroscopy" in Progress in Optics, Vol. II, Ed. E. Wolf, North-Holland, Amsterdam (1967).
"Proc. Aspen International Conference on Fourier Spectroscopy," Ed. by G. Vanasse, A.T. Stair, and D. Baker, AFCRL Special Report No. 114 (1971).

4. "RT-11 System Reference Manual", Digital Equipment Corporation, Maynard, MA, Pub. No. ORUGA-C-D, DN1, DN2 (1976).

5. D.J. Lovell and J. Strong, Appl. Opt. 8, 1673 (1969).

6. D.C. Cartwright *et al*, Phys. Rev. A 16, 1041 (1977).

7. C.E. Moore, NSRDS-NBS 3, Sect. 7, U.S. Government Publication (1976).

8. R. Murphy, F. Cook and H. Sakai, J. Opt. Soc. Am. 65, 600 (1975).
H. Sakai and R. Murphy, Appl. Opt. 17, 1342 (1978).
W. Benesch and K. Saum, J.Q.S.R.T. 12, 1129 (1972).

9. Infrared Emission Spectroscopy was actively engaged by two groups, one headed by W. Benesch and another by K. McCubbin.
W. Benesch and K. Saum, J.Q.S.R.T. 12, 1129 (1972).
K. Saum and W. Benesch, Appl. Opt. 9, 1419 (1970).
K. McCubbin, paper presented at the 33rd Symposium on Molecular Spectroscopy, Ohio State University (1978).

10. General reference to the molecular nitrogen spectroscopic data:

A. Lofthus and P.H. Krupenie, J. Phys. Chem. Ref. Data 6, 113 (1977).

11. The molecular oxygen spectroscopic data are compiled by P.H. Krupenie, J. Phys. Chem. Ref. Data 1, 423 (1972).

12. G. Herzberg, Ref. 2 (1945) and (1966)
The time-resolved data on the CO-CO_2 fluorescence are described in
H. Sakai, Kagaku No Ryoiki, 32, No. 12, 18 (1978).
H. Sakai and R. Murphy, Applied Opt. 17, 1342 (1978).

13. Emission data: T.R. Todd et al, J. Mol. Spec. 62, 201 (1976).

A.W. Mantz and J. Maillard, J. Mol. Spec. 53, 466 (1974).

Time-resolved data: Sakai (1978) and Sakai and Murphy (1978) of Ref. 12.
Benesch and Saum (1972) of Ref. 9.

H_2 quenching on CO Fluorescence:
J. Stricker, J. Chem. Phys. 68, 934 (1978).

14. R. Murphy, J. Chem. Phys. 54, 4852 (1971).
F. Mies, J. Mol. Spec. 53, 150 (1974).
J.P. Maillard, J. Chanville and A.W. Mantz, J. Mol. Spec. 63, 120 (1976).
D. Baker et al, paper presented at Topical Meeting on Atmospheric Spectroscopy held at Keystone, CO (1978).

15. Analysis of NH uv band:

R.N. Dixon, Can. J. Phys. 37, 1171 (1959).
J. Maliget, J. Brion and H. Guenebaut, J. Chem. Phys. (Fr.) 67, 25 (1970).

Reaction of NH to NO:

I. Hansen et al, Chem. Phys. Letters 42, 370 (1976).
N. Mulvihill and L.F. Phillips, Chem. Phys. Letters 35, 327 (1975).

16. Spectral Analysis:

F. Billingsley, J. Mol. Spec. 61, 53 (1976).
P. Kristiansen, J. Mol. Spec. 66, 177 (1977).
R. Dale et al, J. Mol. Spec. 67, 490 (1977).
C. Amiot, R. Bacts and G. Guelachivili, Can. J. Phys. 56, 249 (1978).

Formation Mechanism:

J. Kennealy et al, J. Chem. Phys. 69, 1574 (1978).

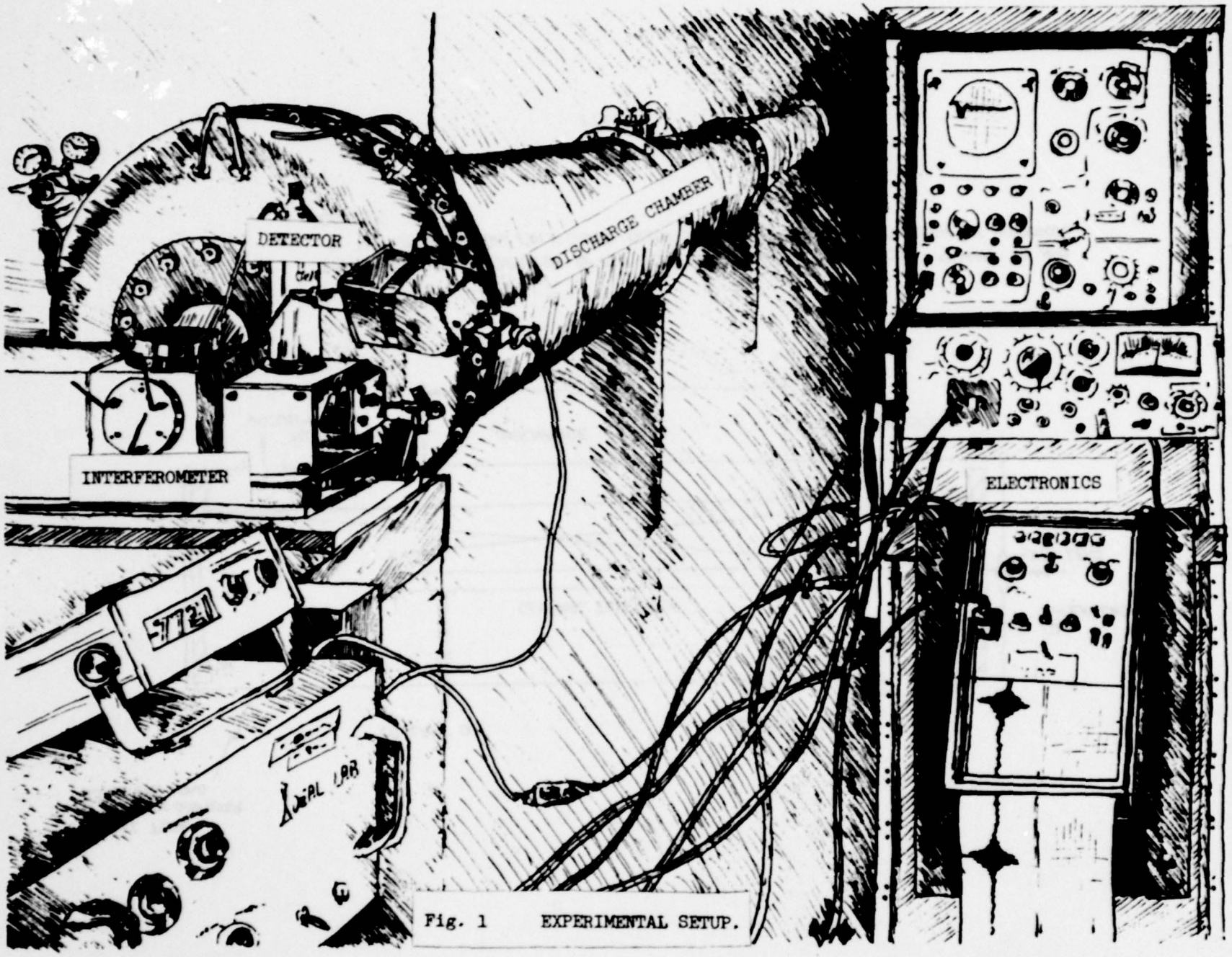

Fig. 1 EXPERIMENTAL SETUP.

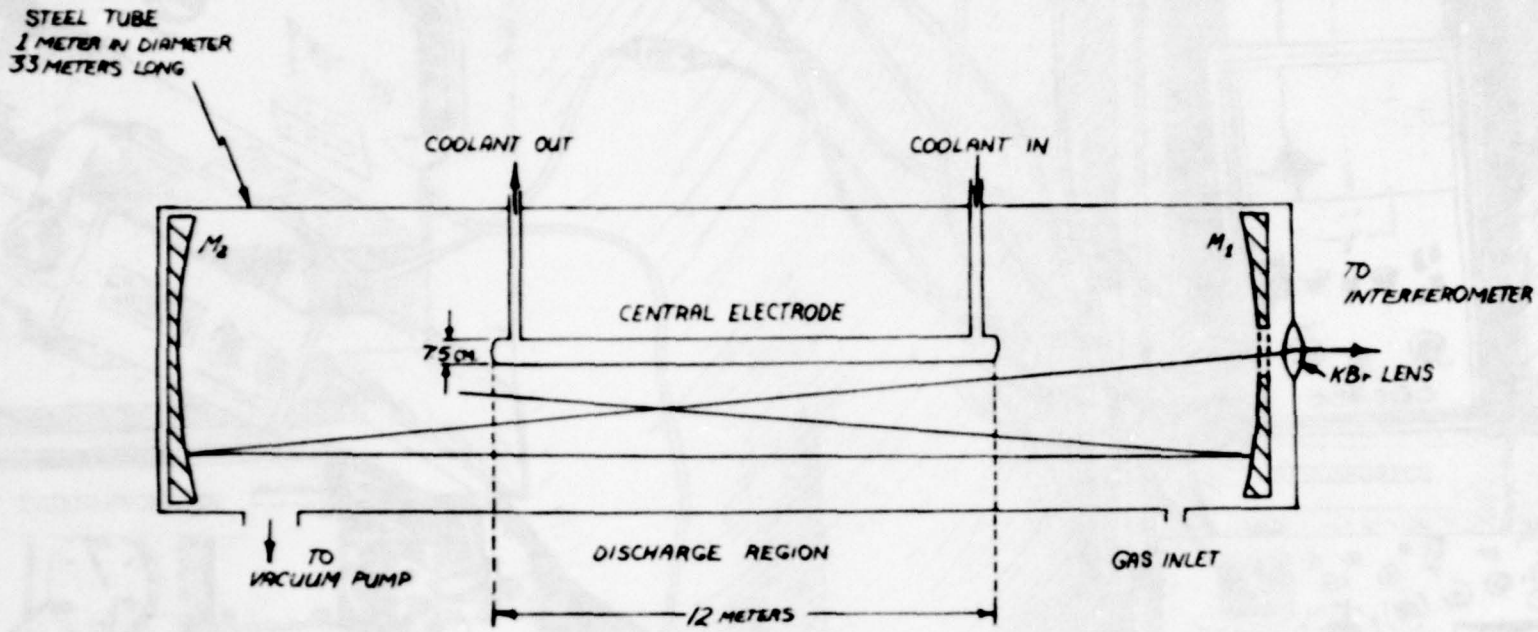

SCHEMATIC REPRESENTATION OF THE DISCHARGE COLUMN (NOT TO SCALE). MIRRORS M_1 AND M_2 ARE FOCUSED ON EACH OTHER RESULTING IN THREE PASSES THROUGH THE DISCHARGE COLUMN.

Fig. 2

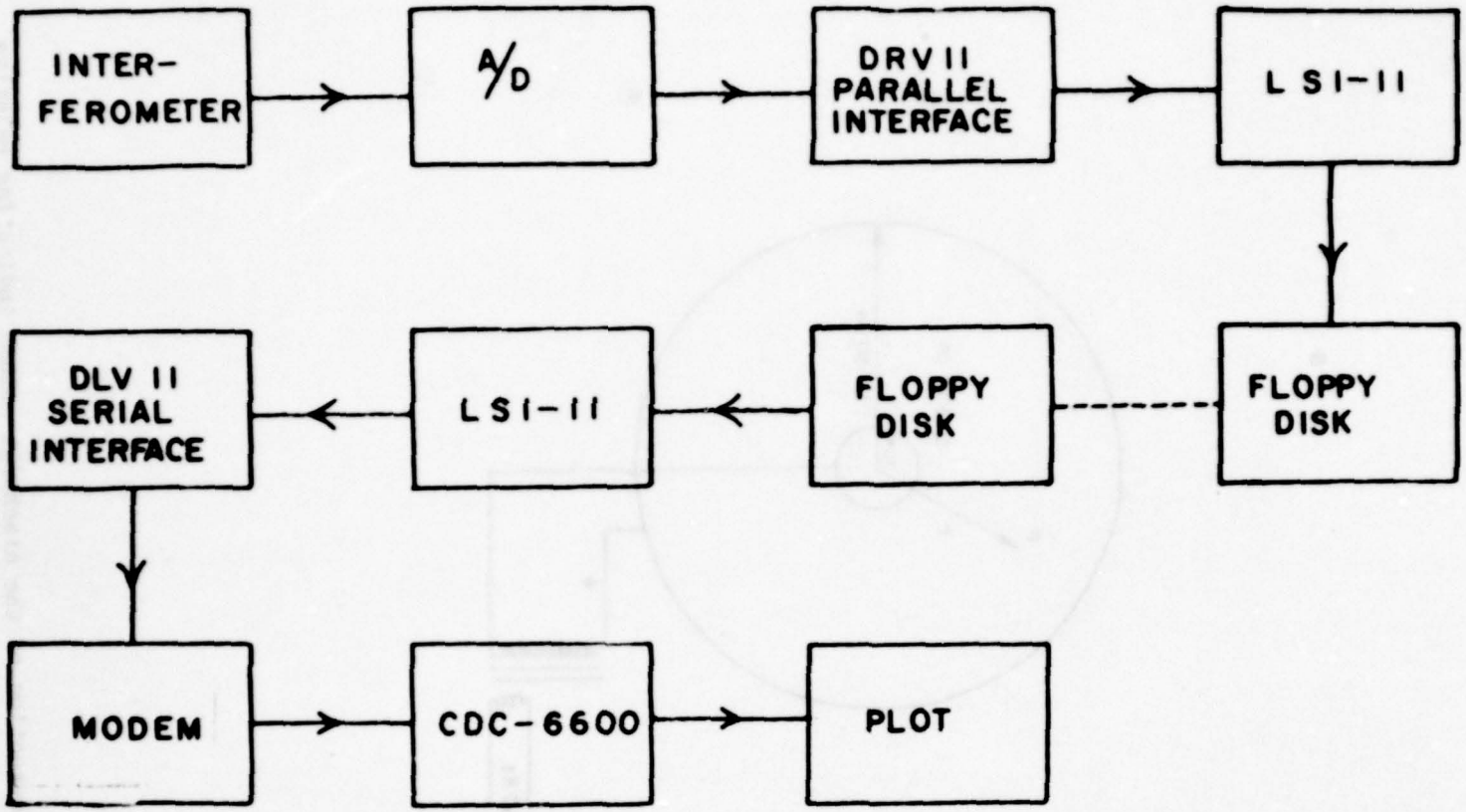

DATA COLLECTION AND PROCESSING SCHEME

Fig. 3

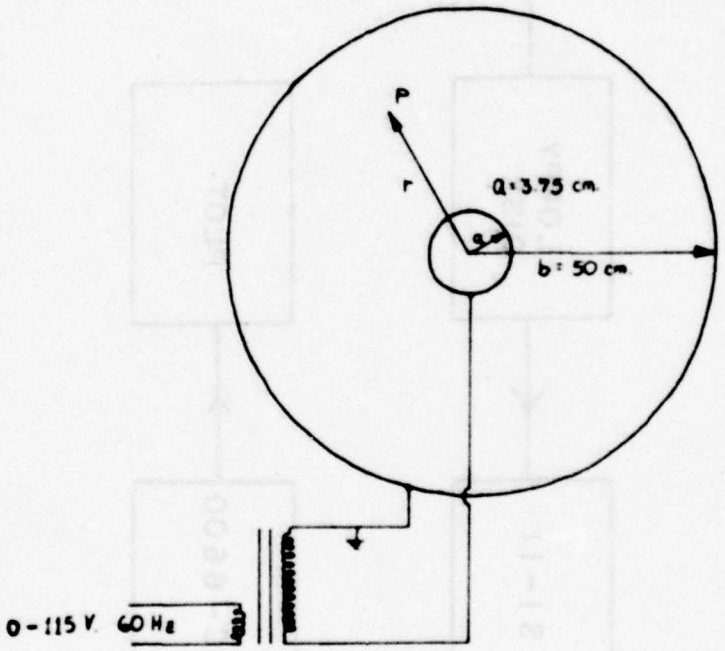

Fig. 4 Cross-section of the discharge column indicating relative dimensions and electrical connections.

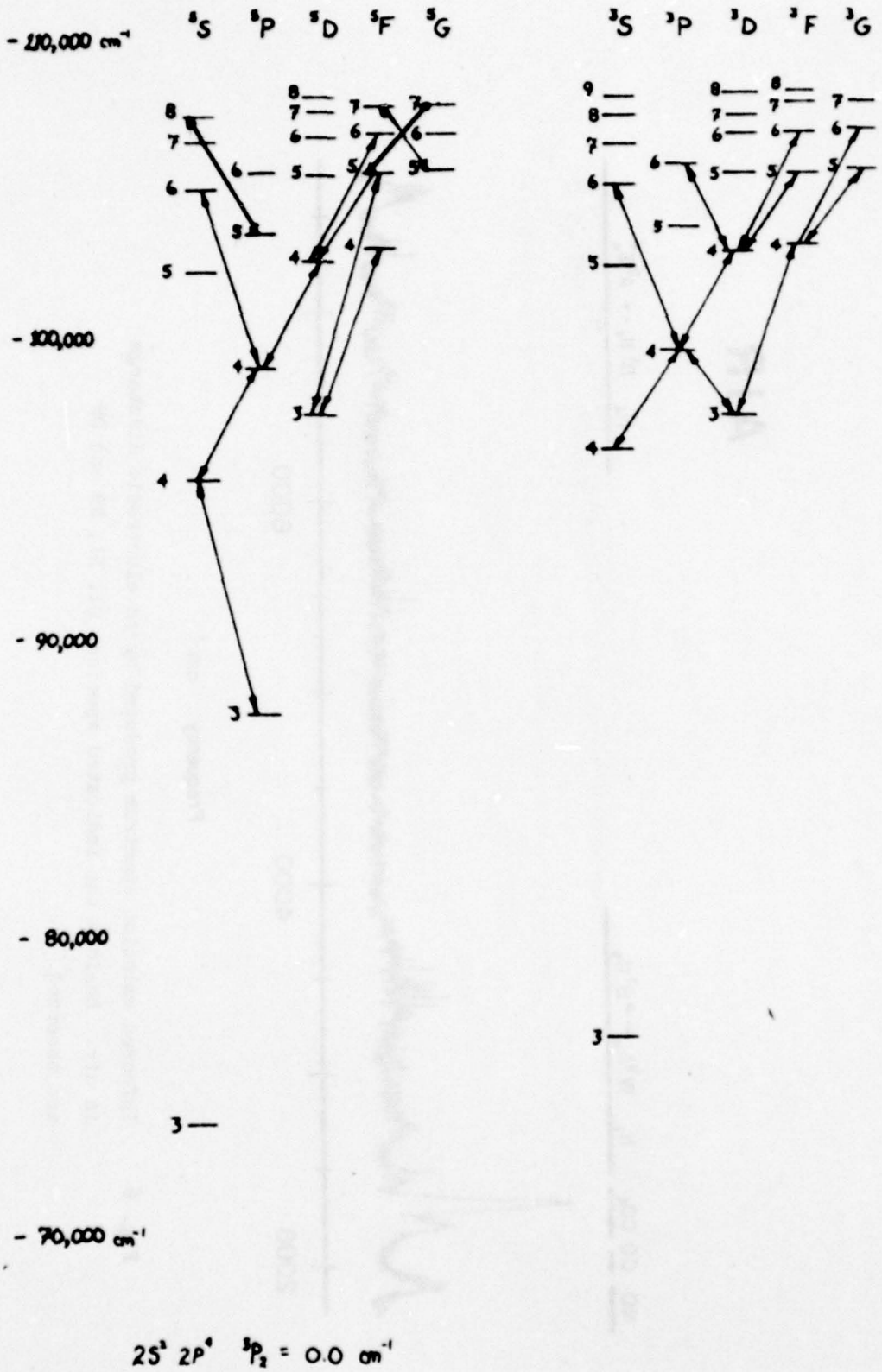

Fig. 5 Energy level diagram of atomic OI indicating observed transitions.

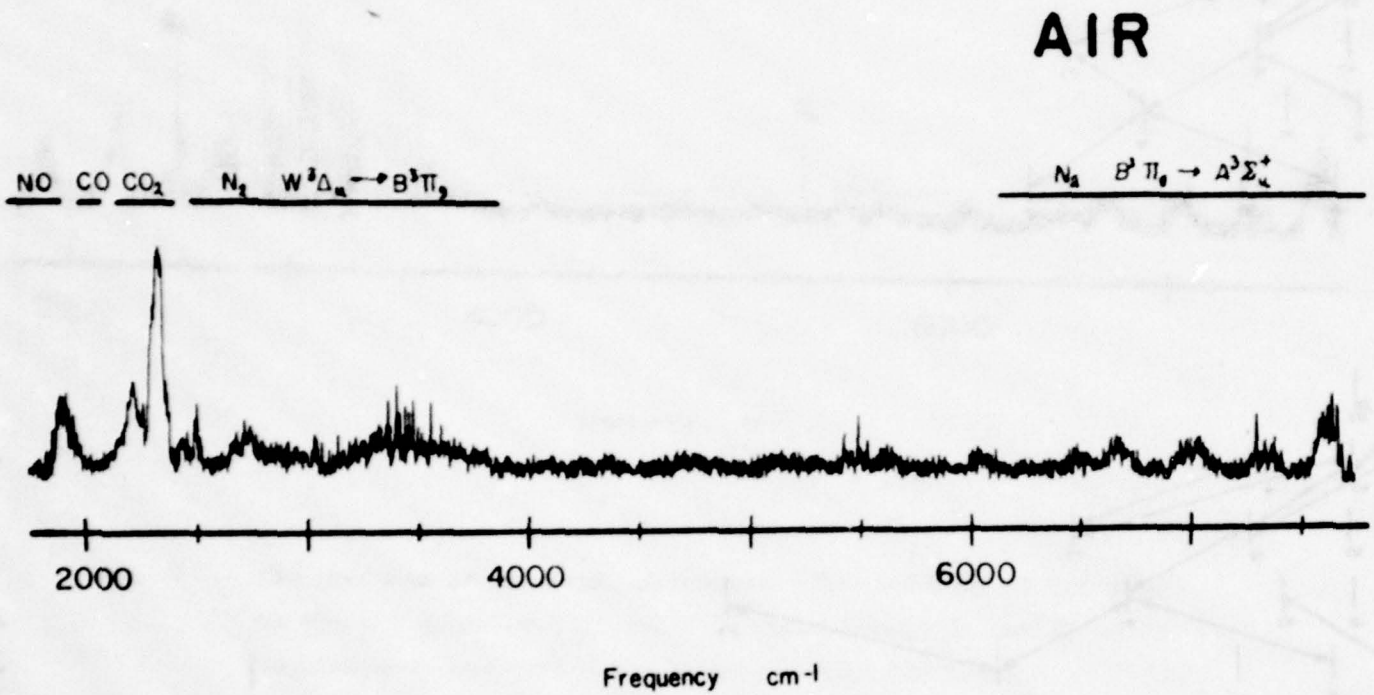

Fig. 6 Infrared emission spectrum produced by an electronic discharge in air. Besides the indicated species, OI, NI, NH and OH are observed.

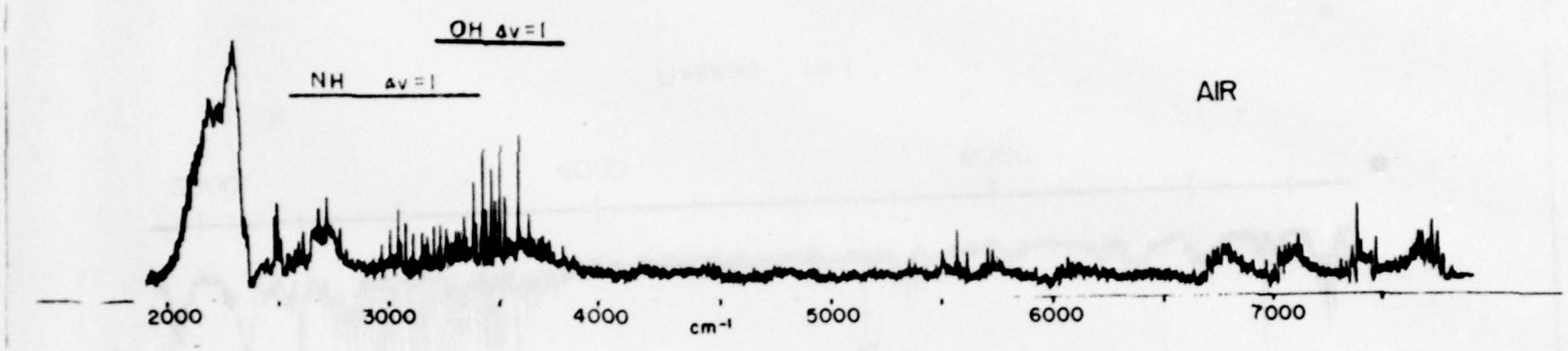

Fig. 7 Spectrum of an air discharge taken at a different time than Fig. 6. The enhanced emission of NH and OH is probably due to a larger moisture content.

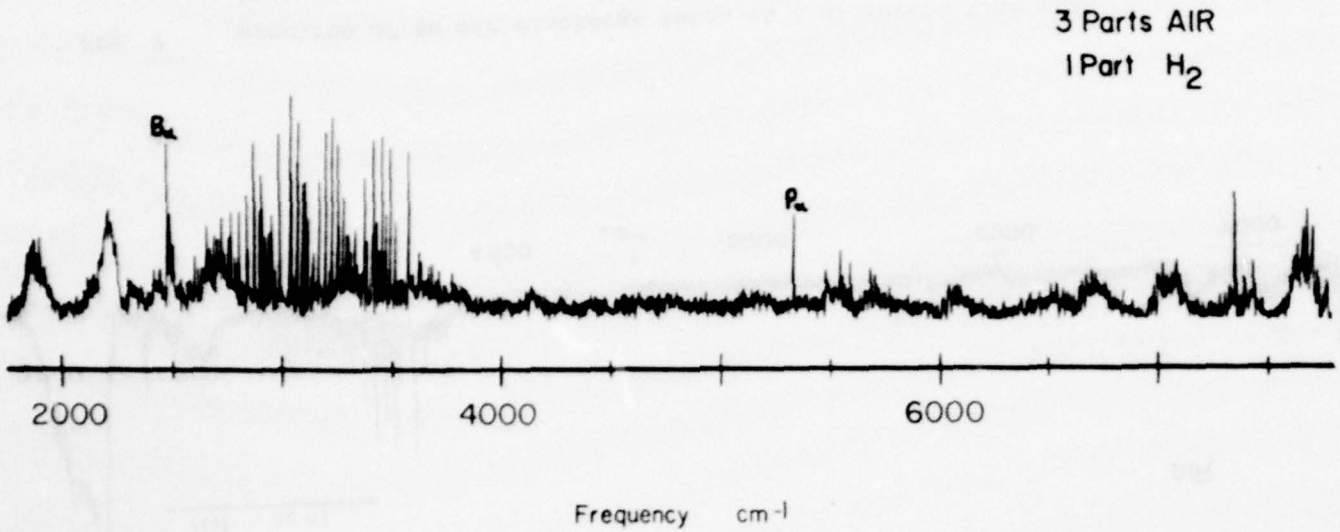

Fig. 8 The spectrum of an air/H_2 discharge. The addition of hydrogen to the air quenches CO_2 $\Delta\nu_3 = 1$ emissions. NH and OH become the dominant emitters. Strong atomic hydrogen lines ($n = 5 \rightarrow 4$) and ($n = 4 \rightarrow 3$) are observed.

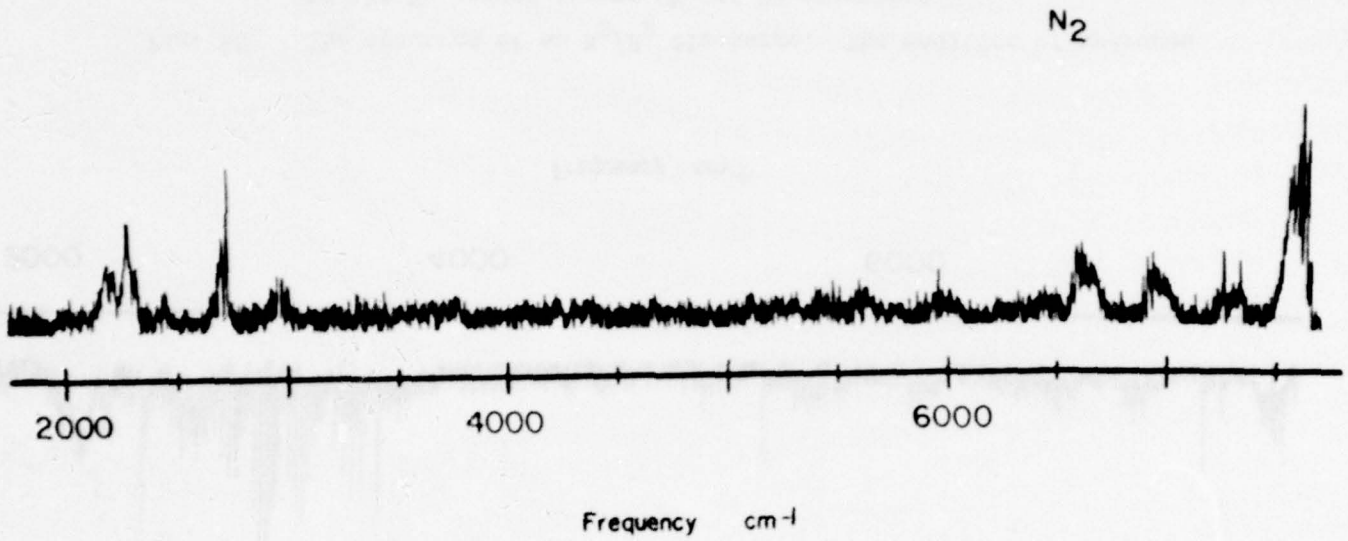

Fig. 9 The spectrum of a N_2 discharge.

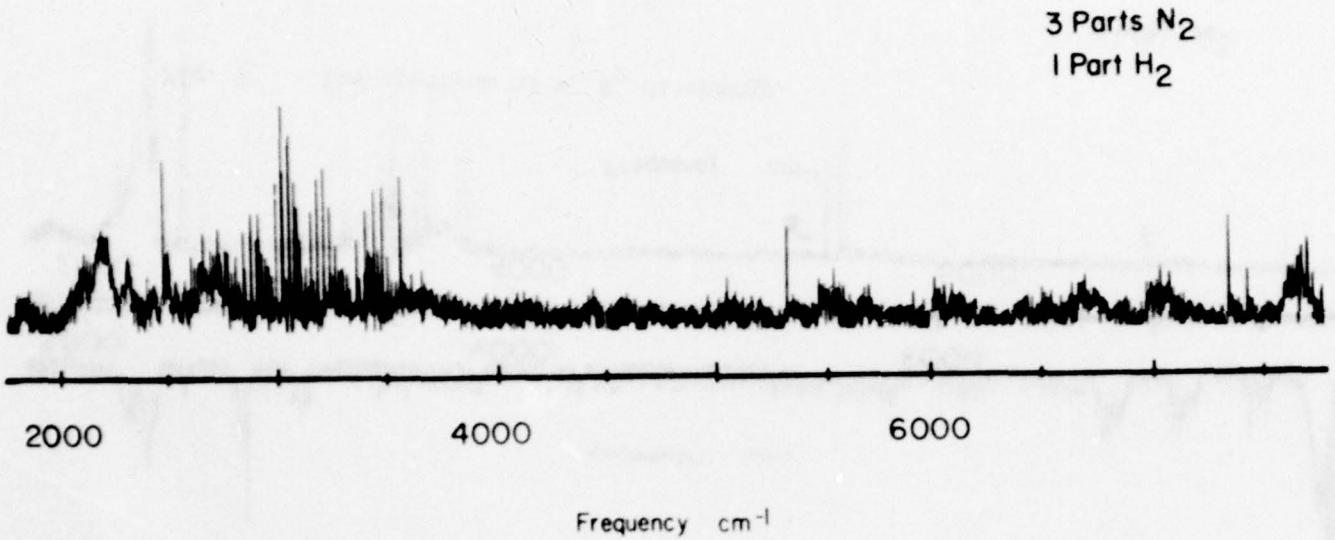

Fig. 10 The spectrum of an N_2/H_2 discharge. The addition of hydrogen to the N_2 causes strong OH and NH emissions.

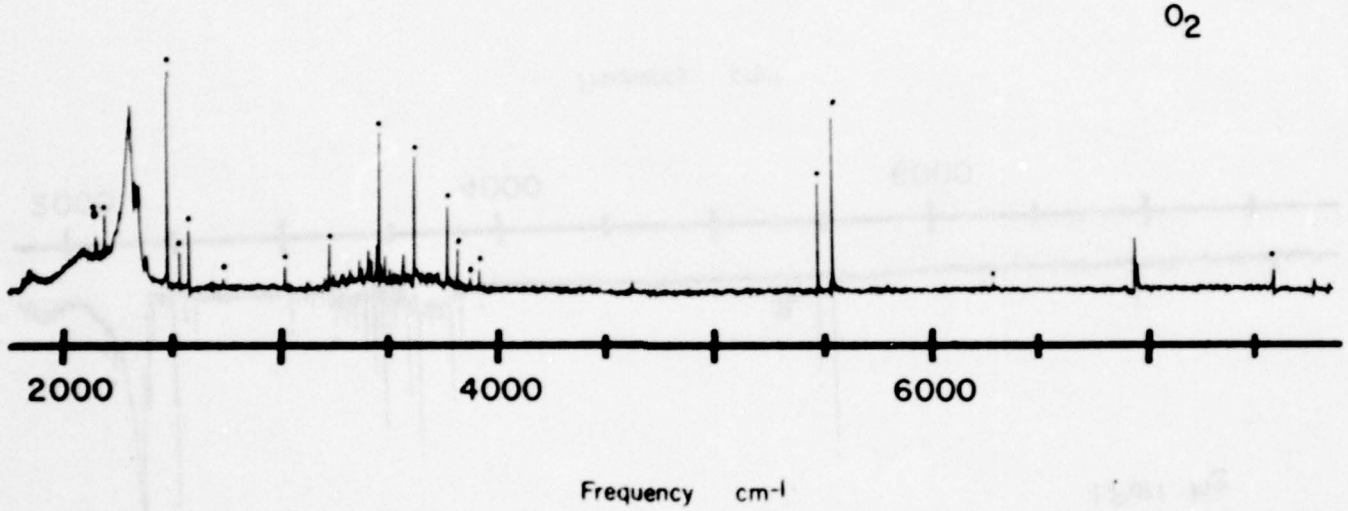

Fig. 11 The spectrum of an O_2 discharge. CO_2 and OI (dotted lines) are the dominant emitters here. The observed OI lines are listed in Table 1.

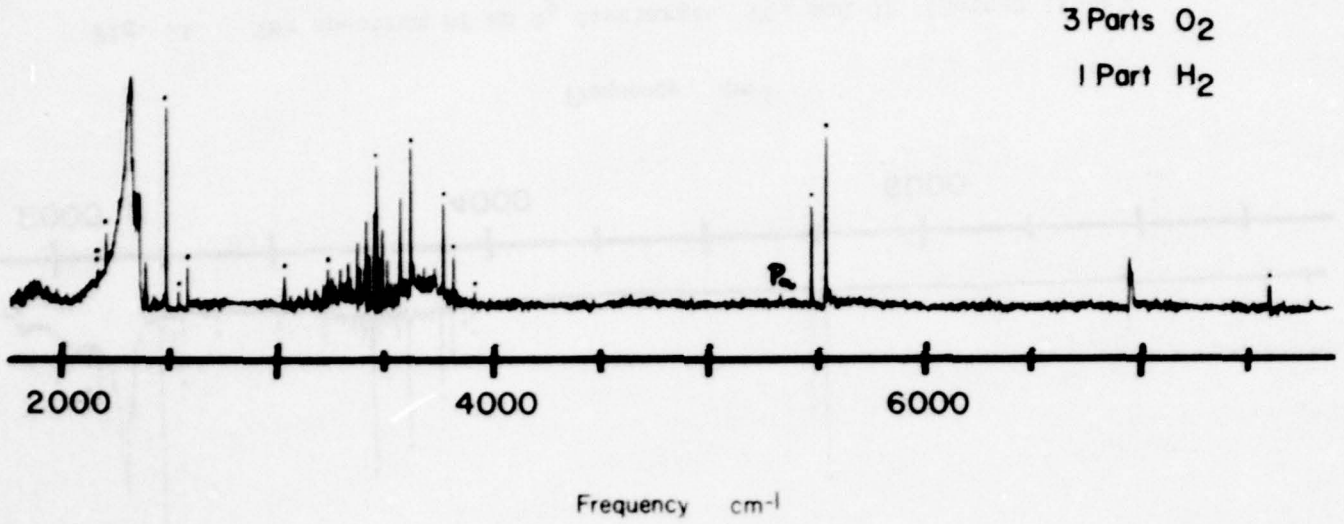

Fig. 12 The spectrum of an O_2/H_2 discharge. The addition of hydrogen causes OH formation. As the atomic hydrogen lines are very weak, most of the hydrogen goes to form OH by recombination.

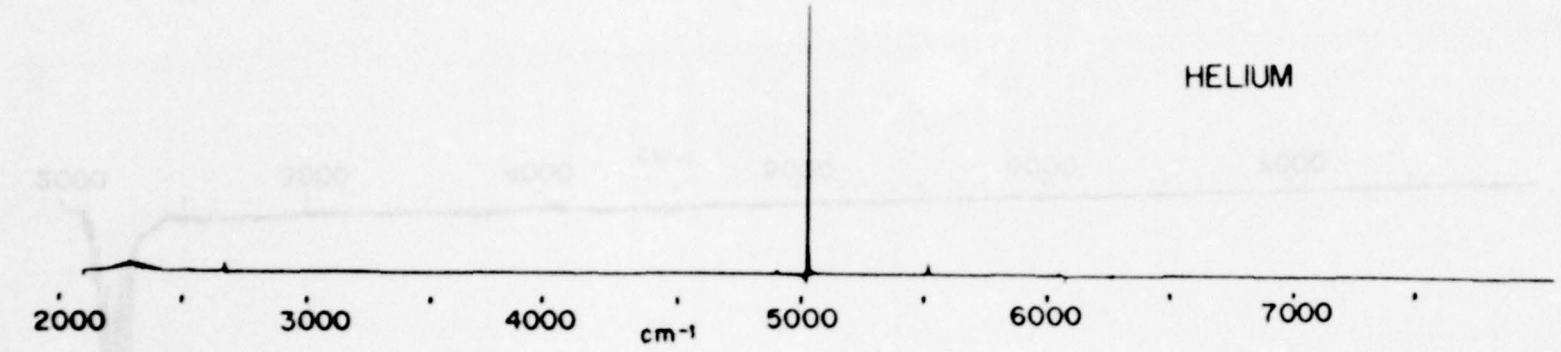

Fig. 13 Spectrum of a He discharge. The dominant feature is the He line at 5117.1 cm^{-1}.

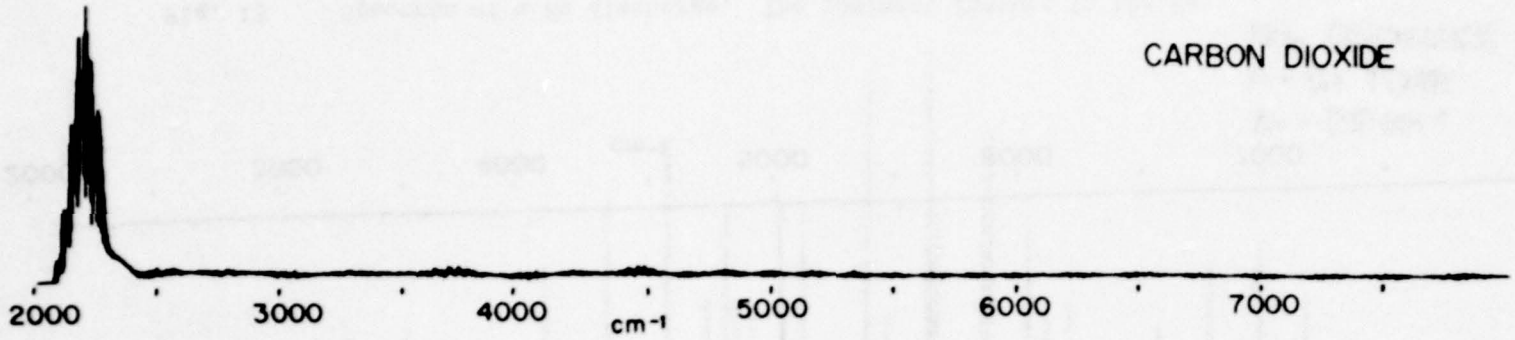

Fig. 14 Spectrum of a CO_2 discharge. CO is the only emitter and no CO_2 emission is observed.

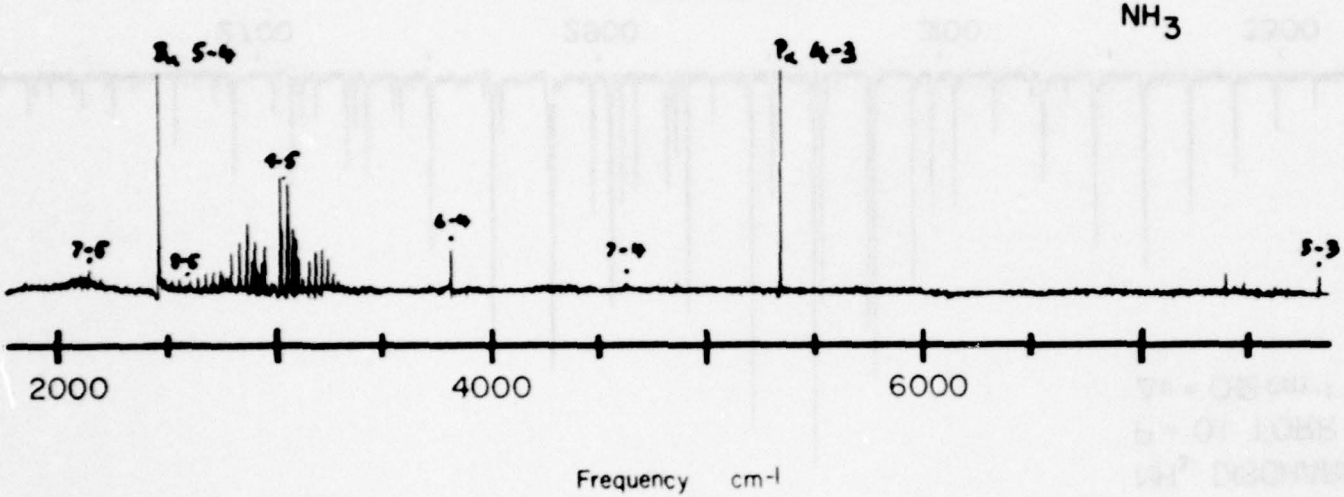

Fig. 15 Emission spectrum produced by an electronic discharge in NH_3. The decomposition products NH and atomic hydrogen (dotted lines) are the observed emitting species. The NH fundamental is well isolated here.

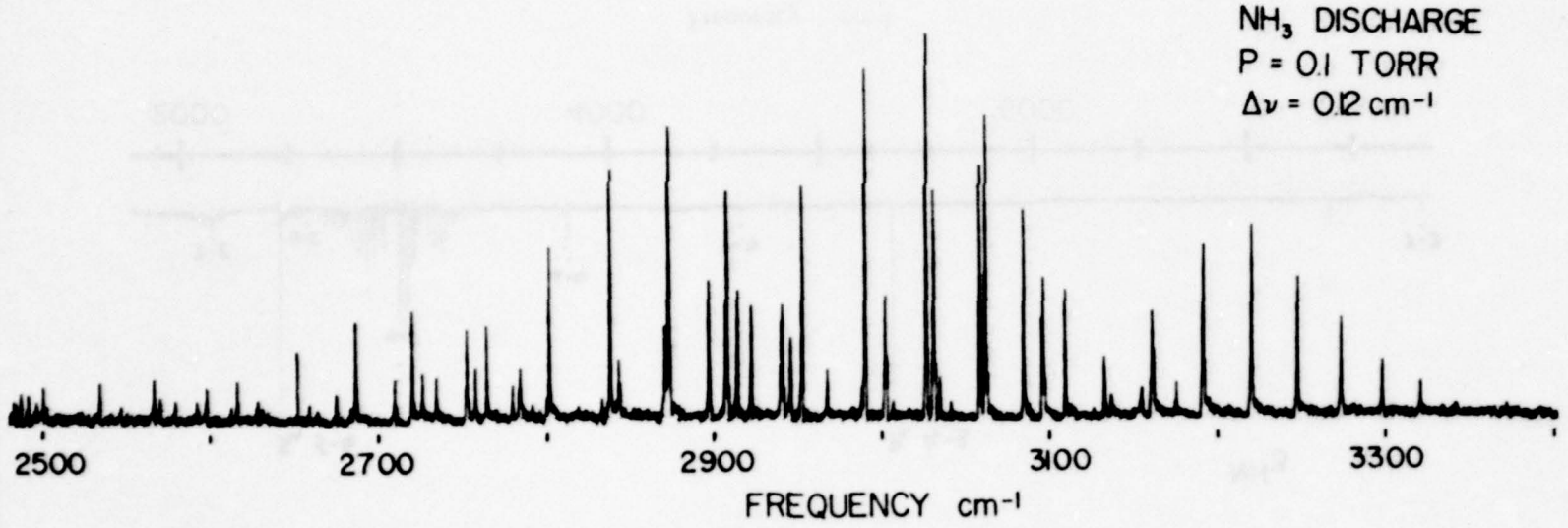

Fig. 16 The NH fundamental observed at higher resolution, $\Delta\sigma = 0.12\ cm^{-1}$.

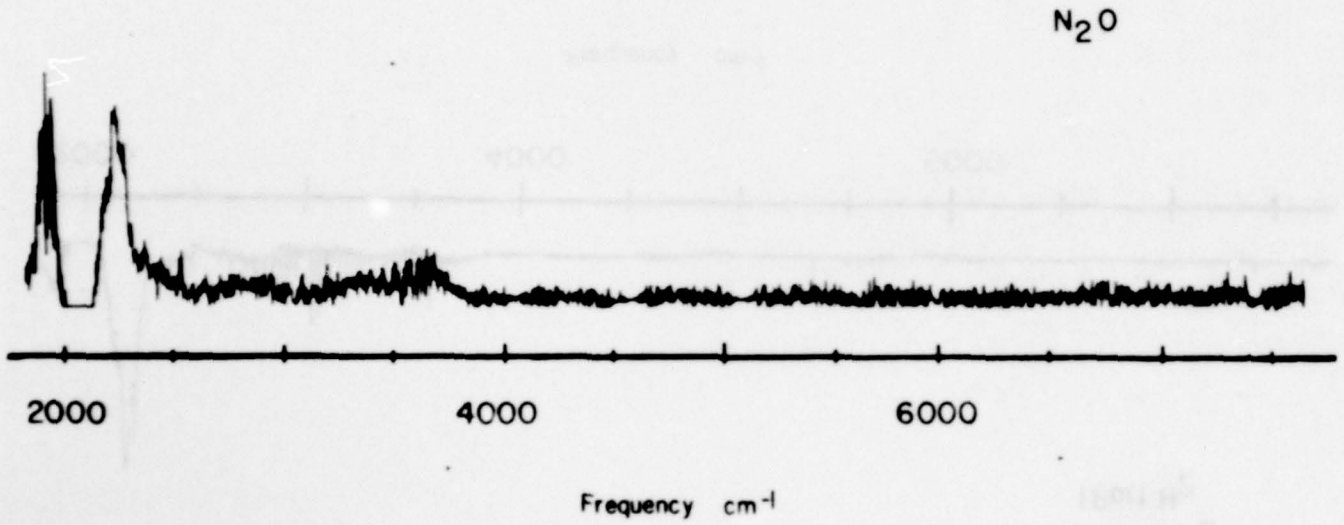

Fig. 17 Spectrum of a N_2O discharge shows NO and CO_2 as strong emitters.

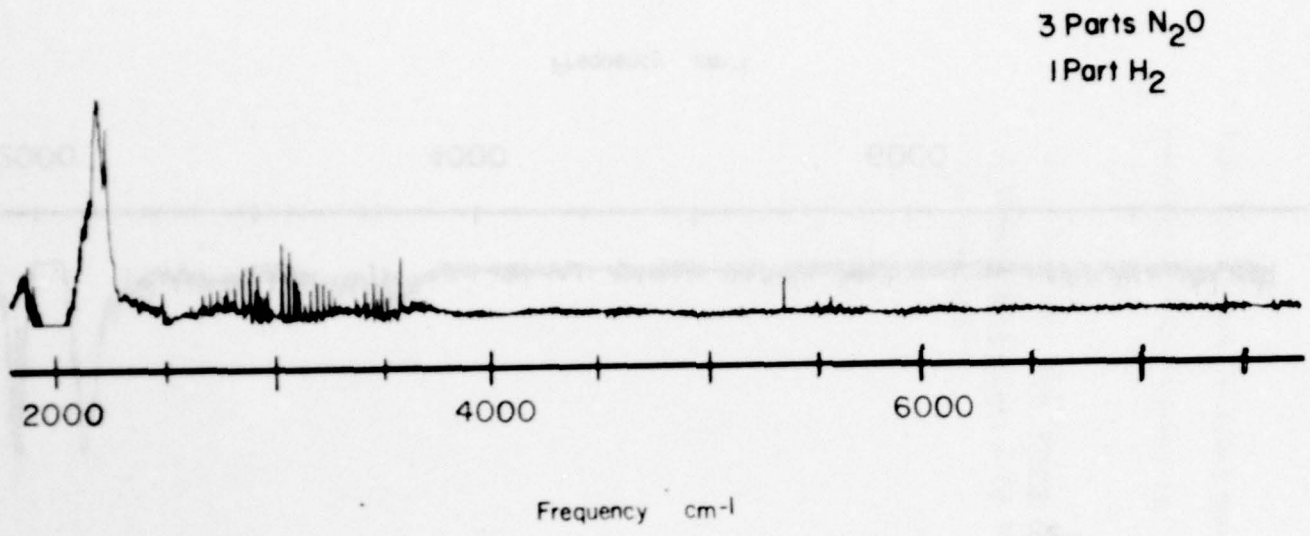

Fig. 18 Spectrum of a N_2O/H_2 discharge. The addition of hydrogen to the N_2O produced significant NH and OH emission while greatly suppressing NO.

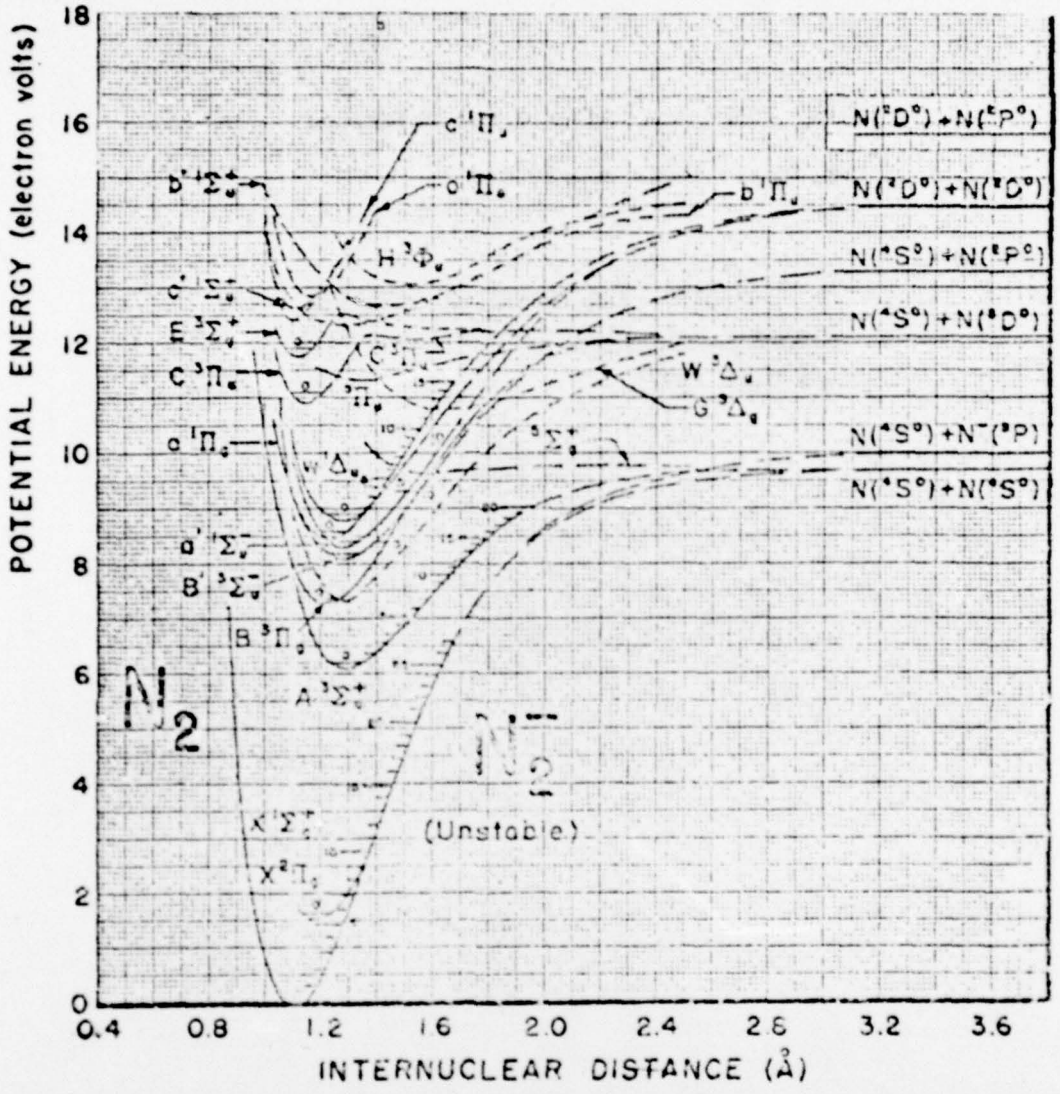

Fig. 19 Potential energy curves for N_2 (after A. Lufthus and P.H. Krupenie, J. Phys. Chem. Ref. Data, 6, 288 (1977).

Figs. 20-23 are included for reference purposes. Their source is:

M. Mizushima, The Theory of Rotating Diatomic Molecules, John Wiley & Sons, New York (1975).

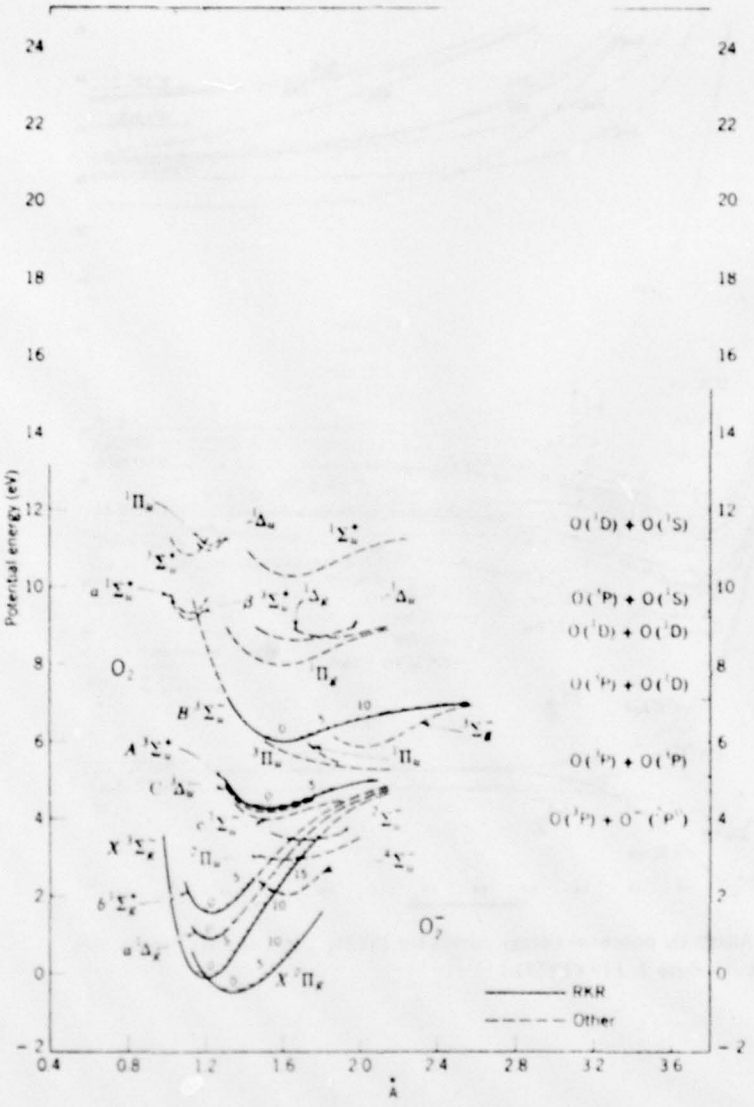

Adiabatic potential energy curves for the O_2^-, O_2.
[P. H. Krupenie, *J. Phys. Chem. Ref. Data* **1**, 423 (1972).]

Fig. 20

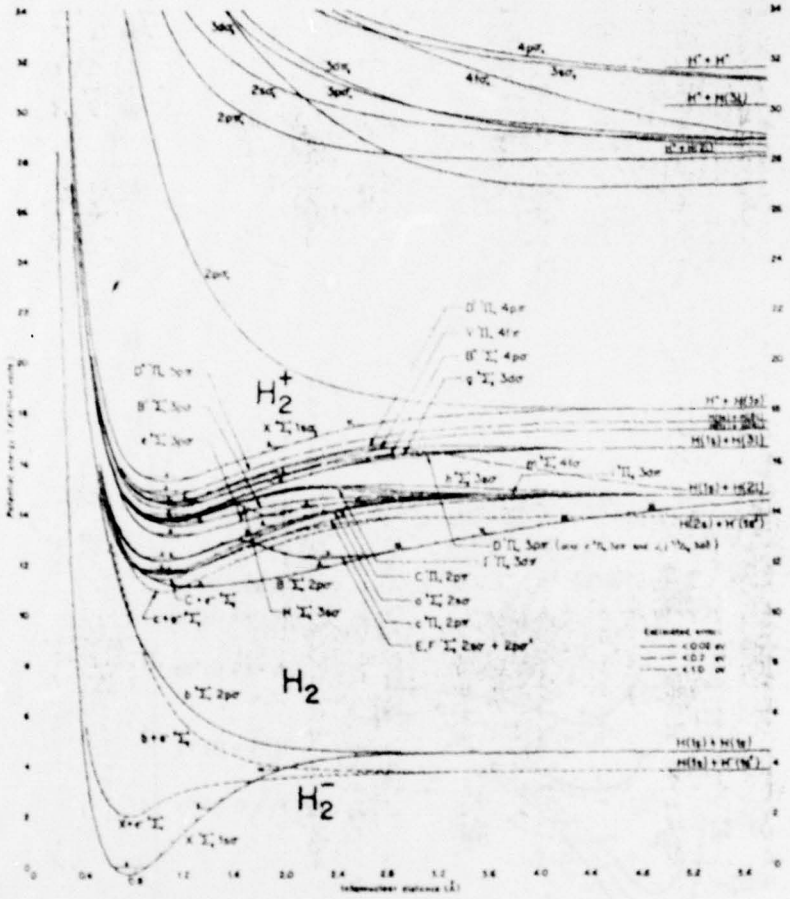

Adiabatic potential energy curves for the H_2^-, H_2, and H_2^+ molecules [T. E. Sharp, *At. Data* 2, 119 (1971).]

Fig. 21

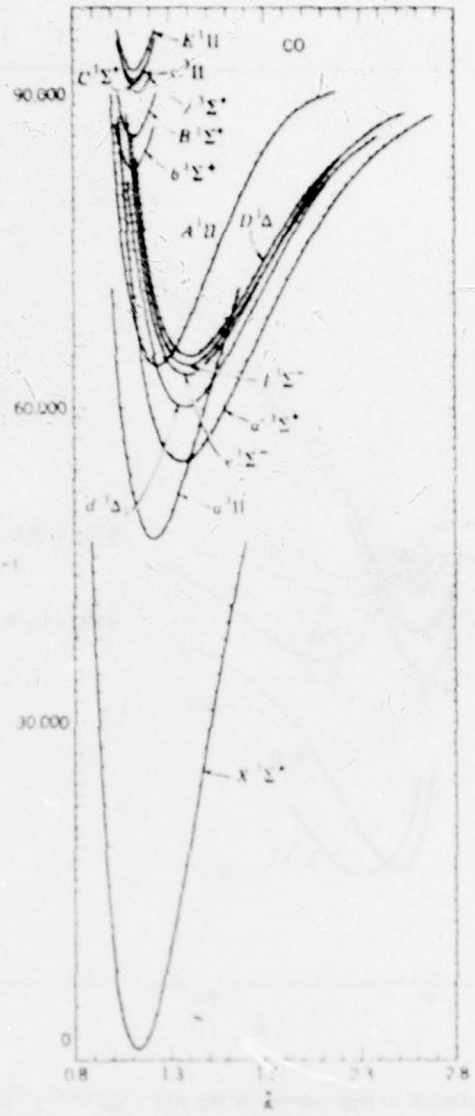

Adiabatic potential energy curves for the CO molecule. [S. G. Tilford and J. D. Simmons, *J. Phys. Chem. Ref. Data* **1**, 147 (1972).]

Fig. 22

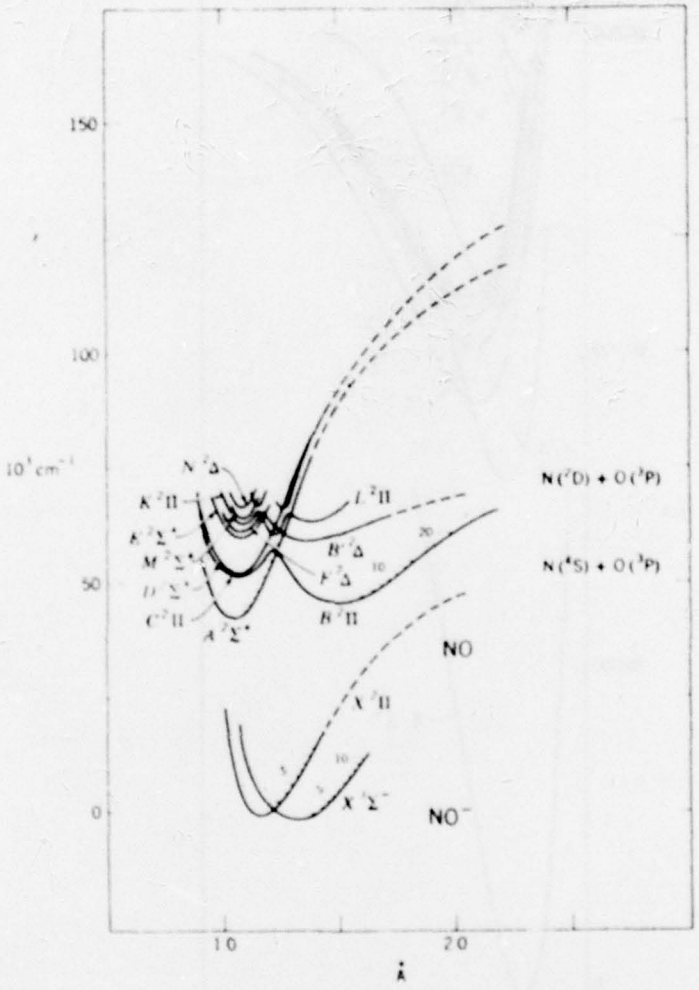

Adiabatic potential energy curves for the NO^-, NO molecules.

[Ch. Jungen, *Can. J. Phys.* **44**, 3197 (1966), A. Lagerqvist and E. Miescher, *Helv. Phys. Acta* **31**, 221 (1958), A. Lagerqvist and E. Miescher, *Can. J. Phys.* **44**, 1525 (1966), K. P. Huber, *Helv. Phys. Acta* **34**, 929 (1961), K. P. Huber, *Can. J. Phys.* **46**, 1691 (1968), D. Spence and G. J. Schulz, *Phys. Rev.* **A3**, 1968 (1971).]

Fig. 23

APPENDIX

This program relays incoming data from the DRV-11 parallel interface to diskette #1

```
        .TITLE  DRV 11 TO DISK

        .CSECT  DRVDX1
        .MCALL  ..V2..,.REGDEF,.TTYIN,.ENTER,.FETCH
        .MCALL  .WRITW,.CLOSE,.PRINT,.EXIT
        .GLOBL  IREA,IOUT


        ..V2..
        .REGDEF
        BLK=R2
        BCOUN=R3

INT:    MOV     R2,SAV  ;INTERRUPT ROUTINE
        MOV     DPT,R2
        CMP     #<1776+B1>,R2
        BGE     NF
        MOV     #B1,R2
NF:     MOV     @#167774,(R2)+
        MOV     R2,DPT
        MOV     SAV,R2
        RTI

START:  .PRINT  #ENCOUN
        JSR     PC,IREA
        MOV     R1,BCOUN
        DEC     BCOUN   ;FIRST BLOCK 0
        .FETCH  #HDX1,#DX1
        BCS     FET
        .ENTER  #AREA,#0,#DX1,#-1
        BCS     ENT
        MOV     #INT,@#304      ;SET UP INTERRUPT
        MOV     #340,@#306
        MOV     #B1,DPT
        MOV     #40,@#167770
        CLR     BLK
A:      CMP     DPT,#B2 ;CHECK TO SEE IF BUFF ONE FULL
        BLT     A

        .WRITW  #AREA,#0,#B1,#400,BLK
        BCS     BWR

        INC     BLK
        CMP     BCOUN,BLK
        BLT     EX
B:      CMP     DPT,#B2 ;CHECK TO SEE IF BUFF TWO FULL
```

```
        BGE     B
        .WRITW  #AREA,#0,#B2,#400,BLK
        BCS     BWR

        INC     BLK
        CMP     BCOUN,BLK
        BGE     A

EX:     BIC     #40,@#167770
        .CLOSE  #0
        .PRINT  #GDRD
        MOV     BLK,R0
        JSR     PC,IOUT
        .EXIT

FET:    .PRINT  #BADFET
        .EXIT

ENT:    .PRINT  #BADENT
        .EXIT

BWR:    .PRINT #BADWR
        .EXIT


GDRD:   .ASCIZ  /NUMBER OF BLOCKS STORED ON DX1:DATA.INT IS:/
BADFET: .ASCIZ  /BAD FETCH/
BADENT: .ASCIZ  /BAD ENTER/
BADWR:  .ASCIZ  /BAD WRITE/
ENCOUN: .ASCIZ  /ENTER NUMBER OF BLOCKS TO BE READ/

B1:     .BLKW   400
B2:     .BLKW   400
AREA:   .BLKW   10

SAV:    .WORD   0
DPT:    .WORD   0

DX1:    .RAD50  /DX1/
        .RAD50  /DAT/
        .RAD50  /A  /
        .RAD50  /INT/

HDX1:   .BLKW   4000
        .END    START
*
```

This is an ASCII character conversion program.

```
        .TITLE  CODE 6-BIT ASCII

        ;OUTPUTS ONE LINE 129 BYTES LONG WITH <CR>
        ;R2 BUFF IN LOCATION
        ;R3 BUFF OUT LOCATION
        ;R3 AFTER RUNNIONG IS SAME AS BEFORE
        ;R2 COULD EQUAL R3

        .CSECT  CODE6
        .GLOBL  COD
        .MCALL  ..V2..,.REGDEF

        ..V2..
        .REGDEF

WOR     =R0
HOLD    =R1

COD:    MOV     R0,-(SP)
        MOV     R1,-(SP)
        MOV     R3,-(SP)

        MOV     #100,COUNT      ;OUTPUT 64 WORDS
LOOP:   MOV     (R2)+,HOLD
        INC     HOLD    ;ZERO IS <EOR> ON CDC
        CMP     #10000,HOLD
        BNE     C
        MOV     #7777,HOLD
C:      MOV     HOLD,WOR
        ASL     WOR     ;HIGH ORDER BYTE
        ASL     WOR
        BIC     #140377,WOR
        SWAB    WOR
        MOVB    TABLE(WOR),(R3)+
```

```
BIC     #177700,HOLD    ;LOW ORDER BYTE
        MOVB    TABLE(HOLD),(R3)+
        DEC     COUNT
        BGT     LOOP

        MOVB    #15,(R3)+       ;OUTPUT <CR>

        MOV     (SP)+,R3
        MOV     (SP)+,R1
        MOV     (SP)+,R0
        RTS     PC

COUNT:  .WORD   0
TABLE:  .ASCII  /:ABCDEFGHIJKLMNOPQRSTUVWXYZ0123456789+-*/
        .BYTE   57
        .ASCII  /()$= ,.#[]%'_!&'?<>@\^;/

        .END
*
```

This program transmits data on diskette #1 to the central CDC facility via modem.

```
        .TITLE  DISK TO CDC
        .CSECT  DX1CDC
        .MCALL  ..V2..,.REGDEF,.LOOKUP,.FETCH,.PRINT,.EXIT,.READW
        .GLOBL  IREA,IOUT,COD


        ..V2..
        .REGDEF
        COUNT=R4
        BLK=R5

TXCSR   =177564
TXBUFF  =177566

MRCSR   =175610
MRBUFF  =175612
MXCSR   =175614
MXBUFF  =175616


START:  .PRINT  #ENCOUN
        JSR     PC,IREA
        MOV     R1,BCOUN
        DEC     BCOUN    ;FIRST BLOCK 0
        .FETCH  #HDX1,#DX1
        BCS     FET
        .LOOKUP #AREA,#0,#DX1
        BCS     ENT
        CLR     BLK

A:      .READW  #AREA,#0,#B1,#400,BLK
        BCS     BAREA
        MOV     #400,COUNT
        MOV     #B1,R2

        MOV     #4,LCOU          ;OUTPUT 4 LINES
SL:     MOV     #BOUT,R3

        JSR     PC,COD

T:      BIT     #200,MXCSR       ;SEND ONE CHAR
        BEQ     T
        MOVB    (R3),MXBUFF
R:      BIT     #200,MRCSR       ;READ ECHO
        BEQ     R
        MOV     MRBUFF,TEM

        CMPB    TEM,(R3)+        ;CHECK FOR ERROR
        BNE     ER

        CMPB    #15,TEM ;LOOK FOR <CR>
        BNE     T
```

```
        MOV     #12,ZCOU        ;WAIT 10'TH CHAR SHOULD BE ?
RCR:    BIT     #200,MRCSR
        BEQ     RCR
        CMP     #77,MRBUFF      ;CHECK FOR ?
        BEQ     RSP
        DEC     ZCOU
        BGT     RCR
        BR      ERE

FET:    .PRINT  #BADFET
        .EXIT

ENT:    .PRINT  #BADENT
        .EXIT

BAREA:  .PRINT  #BADREA
        .EXIT

RSP:    BIT     #200,MRCSR      ;CHECK FOR <SP>
        BEQ     RSP
        CMP     #240,MRBUFF
        BNE     ERE

        DEC     LCOU
        BGT     SL
        INC     BLK
        CMP     BCOUN,BLK
        BGE     A
TCR:    BIT     #200,MXCSR      ;SEND   <CR>
        BEQ     TCR
        MOV     #15,MXBUFF

        .PRINT  #GOOD
        .EXIT

ER:     DEC     R3              ;AN ERROR HAS OCCURRED
TBC:    BIT     #200,MXCSR
        BEQ     TBC
        MOVB    #10,MXBUFF      ;SEND   <BS>
RBC:    BIT     #200,MRCSR
        BEQ     RBC
        CMP     #210,MRBUFF     ;CHECK ECHO <BS>
        BEQ     T
ERE:    .PRINT  #EREX
        .EXIT
```

```
BADFET: .ASCIZ  /BAD FETCH/
BADENT: .ASCIZ  /BAD LOOKUP/
BADREA: .ASCIZ  /BAD DISK READ/
ENCOUN: .ASCIZ  /ENTER NUMBER OF BLOCKS TO BE READ/
EREX:   .ASCIZ  / ERROR EXIT /
GOOD:   .BYTE   7       ;BELL
        .ASCII  / GOOD TRANSFER!!/
        .BYTE   7
        .BYTE   0

        .EVEN
BCOUN:  .WORD   0
LCOU:   .WORD   0
BOUT:   .BLKW   300
ZCOU:   .WORD   0
TEM:    .WORD   0
B1:     .BLKW   400
AREA:   .BLKW   10

SAV:    .WORD   0
DPT:    .WORD   0

DX1:    .RAD50  /DX1/
        .RAD50  /DAT/
        .RAD50  /A  /
        .RAD50  /INT/

HDX1:   .BLKW   4000
        .END    START

*
```